Journal of Ambient Intelligence and Humanized Computing
https://doi.org/10.1007/s12652-019-01416-w

ORIGINAL RESEARCH

A smart brain MR image completion method guided by synthetic-CT-based multimodal registration

Jiamin Zheng[1] · **Kaijian Xia**[2] · **Qiankun Zheng**[1] · **Pengjiang Qian**[1]

Received: 14 May 2019 / Accepted: 23 July 2019

Abstract
We propose a novel method for brain MR image completion in the case of unknown deformation in MR images. An efficient technique for MR image completion can keep patients from requiring a secondary shot, thus limiting radiation exposure. To address this challenge, we propose an MR image completion method guided by multimodal registration and simultaneously propose a new multimodal registration method, i.e., synthetic-CT-based multimodal registration (IC-G-MR). The majority of existing multimodal registration methods cannot perform well under the conditions mentioned above. The significance of our method can be summarized as follows: (1) Through a combination of transfer learning and indirect multimodal registration, the proposed IC-G-MR method can be used to solve the problem of brain MR image completion based on corresponding normal CT images. (2) Due to the transfer learning technique, our method can generate synthetic brain CT images of good quality. (3) Due to the novel multimodal registration method, the proposed IC-G-MR method performs effectively in registration for large-scale elastically deformed MR images. The experimental results indicate that our proposed IC-G-MR method can effectively complete MR images of the brain.

Keywords Smart diagnosis · Image completion · Synthetic CT generation · Transfer learning · Multimodal registration

1 Introduction

With the development of medical imaging technology and intelligent diagnosis in recent years, medical images of various modalities, e.g., CT, MRI, and PET, have been extensively used to observe the tissue and bone morphology inside the human body, especially for clinical diagnosis (Manchanda and Sharma 2018; Yang et al. 2008; Alafeef and Fraiwan 2019). Notably, images of different modalities provide different information. For example, MR and CT images show excellent anatomical information and precise skeletal location information, whereas PET images provide functional information that enables the detection of metabolic abnormalities.

Currently, most existing methods for image completion are designed to fill in damaged images (Iizuka et al. 2017; Chen et al. 2019). In medical image processing, deep learning has been adopted to correct noisy data (Guo et al. 2019). MRI is commonly used to examine the organs for abnormalities so that we can detect diseases such as brain tumour (Raja et al. 2018; Sharif et al. 2018). In clinical application scenarios, MR images may be contaminated or damaged due to the presence of an abnormal magnetic field during image acquisition, which will cause unknown deformation in the MR images. However, proper diagnosis requires normal medical images. Thus, the question arises: what are the characteristics of a normal MR image? The major challenge faced is to determine the correct approach to take for image completion. To put it simply, for compromised MR images, a way to clearly assess the validity of the final results obtained is needed. In other words, some guidance, such as an atlas, may be necessary during the image completion process to ensure its correctness. In addition, MR images acquired from different individuals exhibit marked differences, and the generalizability of typical atlases is not satisfactory. Therefore, finding appropriate guidance for this purpose is our priority.

✉ Kaijian Xia
xiakaijian@163.com

[1] School of Digital Media, Jiangnan University, 1800 Lihu Avenue, Wuxi 214122, Jiangsu, People's Republic of China

[2] Soochow University Changshu Hospital, Changshu No 1 People's Hospital, Changshu 215500, Jiangsu, People's Republic of China

Published online: 01 August 2019

To address this challenge, inspired by the aggregation of information from medical images of different modalities, we utilize normal CT scans from the same patient as a guide to repair MR images. A novel MR image completion method guided by multimodal registration is proposed to solve this problem. Thus, our method is not merely image completion in the traditional sense. Based on corresponding CT scans for the same patient, the proposed method aims to repair MR images such that they will be highly consistent with the CT scans. In other words, our method can simultaneously repair deformed MR images and register them with respect to corresponding CT scans for further diagnosis.

Images from different modalities always exhibit significant variations; consequently, multimodal registration is more difficult to perform than monomodal registration. Various methods have been proposed to solve the problem of multimodal registration, such as methods based on mutual information (Fernandez-de-Manuel et al. 2014), elastodynamics (Ahmad and Khan 2018), and feature points (Alvén et al. 2016). However, many of these methods are voxel-based methods, which are disadvantageous in terms of computational complexity and are difficult to apply in the clinic (Xue and Tang 2014; Akhbardeh et al. 2015; Lee et al. 2010).

The method we propose is called MR image completion guided by synthetic-CT-based multimodal registration (IC-G-MR). Concerning synthetic CT generation, there are several existing methods for this purpose, such as atlas-based (Hofmann et al. 2008; Farjam et al. 2019), template-based (Kops and Herzog 2008), and model-based segmentation (Zaidi et al.2003) methods. Actually, medical segmentation have already greatly used in clinical practice (Han et al. 2018). The greatest difficulty here lies in differentiating bone and air in MR images due to their low signals (Keereman et al. 2010).

For more effective clinical application, the principal ideas adopted in our method are transfer learning and indirect multimodal registration. Aiming at the completion of MR images of the brain, the IC-G-MR method offers the following three contributions:

(1) IC-G-MR addresses the problem of brain MR image completion based on pairs of CT images and MR images through a combination of a transfer learning algorithm, i.e., knowledge-transfer-oriented c-means (KT-CM) (Qian et al. 2016), and an indirect multimodal registration approach, i.e., synthetic-CT-based multimodal registration.
(2) Through the use of transfer learning in our method, we can generate better synthetic CT results for the brain using only MR images, thus greatly facilitating the following steps.
(3) Due to the novel multimodal registration method applied, the proposed IC-G-MR method performs effectively in registration for large-scale elastically deformed MR images.

The remaining four sections of the manuscript are organized as follows. The details of related work, i.e., fuzzy c-means (FCM) and KT-CM, are introduced in Sect. 2. The proposed method is presented in Sect. 3. Experimental studies are reported in Sect. 4, along with results and discussions. Conclusions are presented in Sect. 5.

2 Related work

In this section, we introduce the classical soft partition algorithm (FCM) and the transfer learning algorithm (KT-CM) that are adopted in our proposed IC-G-MR method. KT-CM simultaneously inherits the advantages of existing clustering methods and can effectively distinguish air from bone in MR images.

2.1 FCM

FCM (Wen et al. 2018), the classical clustering algorithm, attempts to divide data into disjoint clusters. Let $X = \{x_j | x_j \in R^d, j = 1, \ldots, N\}$ denote a dataset containing N data instances, where d is the dimensionality of the data. Suppose that $C(1 < C < N)$ denotes the number of clusters in the dataset. The framework of FCM can be expressed as follows:

$$\min_{\mathbf{V},\mathbf{U}} \left(J_{FCM}(\mathbf{V},\mathbf{U}) = \sum_{i=1}^{C}\sum_{j=1}^{N} u_{ij}^{m} \left\| \mathbf{x}_j - \mathbf{v}_i \right\|^2 \right), \quad s.t.\ 0 \le u_{ij} \le 1 \ and \ \sum_{i=1}^{C} u_{ij} = 1, \tag{1}$$

where $\mathbf{V} = \{v_i | v_i \in R^d, i = 1, \ldots, C\}$ denotes the cluster centroid matrix, $U \in R^{C \times N}$ represents the membership matrix, and $m > 1$ is a constant.

Through augmented Lagrange optimization, we can update the cluster centroids v_i and the membership values u_{ij} using Eq. (1), as follows:

$$\mathbf{v}_i = \frac{\sum_{j=1}^{N} u_{ij}^{m} x_j}{\sum_{j=1}^{N} u_{ij}^{m}}, \quad i = 1, 2, \ldots, C \tag{2}$$

$$u_{ij} = \frac{1}{\sum_{k=1}^{C} \left(\frac{\|x_j - v_i\|}{\|x_j - v_k\|} \right)^{\frac{2}{m-1}}}, \quad i = 1, 2, \ldots, C; j = 1, 2, \ldots, N \tag{3}$$

2.2 KT-CM

Soft-partition clustering algorithms such as FCM and maximum entropy clustering (MEC) (Tao et al. 2019) are widely used to divide data instances into multiple disjoint clusters. Quadratic weights and Gini-Simpson diversity-based fuzzy clustering (QWGSD-FC), which combines the advantages of the existing methods mentioned above, is a strong soft-partition clustering algorithm.

However, in certain special cases, traditional soft-partition clustering algorithms may not be sufficiently effective. To solve this problem, a combination of transfer learning and conventional soft-partition clustering has been proposed. The transfer learning technique enables the use of prior information from the source domain as a reference for data in the target domain.

Suppose that $X_T = \{x_{1,T}, \ldots x_{N_T,T}\} \in R^{N_T \times d}$ is the data set in the target domain, which contains N_T data instances and has d feature dimensions. The number of clusters is denoted by C_T. $U_T = [u_{ij,T}]_{C_T \times N_T}$ denotes the generated membership matrix, whose elements indicate the membership degree of each data instance $x_j(j = 1, \ldots, N_T)$ with respect to cluster $i(i = 1, \ldots, C_T)$.

The framework of KT-CM can be expressed as follows:

$$\min\left(\begin{array}{l} J_{KT-CM}(V_T, U_T) = \sum_{i=1}^{C_T}\sum_{j=1}^{N_T} u_{ij,T}^2 \left\|x_{j,T} - v_{j,T}\right\|^2 \\ +\beta \sum_{i=1}^{C_T}\sum_{j=1}^{N_T} u_{ij,T}^2 + \gamma \sum_{i=1}^{C_T}\sum_{j=1}^{N_T} u_{ij,T}^2 \|\hat{v}_{i,S} - v_{i,T}\|^2 \end{array}\right) \quad (4)$$

$$s.t. 0 \le \mathrm{u}_{ij} \le 1, \sum_{i=1}^{C_T} u_{ij,T} = 1,$$

where $\beta > 0$ denotes the coefficient of the Gini-Simpson diversity measure, $\gamma \ge 0$ denotes the transfer optimization coefficient, $\hat{v}_{i,S}$ represents the centroid of the *ith* cluster in the source domain, and $v_{j,T}$ represents the estimated centroid of the *jth* cluster in the target domain.

Equation (4) contains three terms. The first term attempts to divide the data instances into C clusters. The second term, derived from the Gini-Simpson index, pursues unbiased probability assignments. The last term is the transfer learning term, the purpose of which is to flexibly draw historical knowledge from the source domain.

The iterative formulas for the cluster centroids and fuzzy membership values are as follows:

$$v_i = \frac{\sum_{j=1}^{N} u_{ij}^2 x_j + \gamma \hat{v}_i \sum_{j=1}^{N} u_{ij}^2}{(1+\gamma)\sum_{j=1}^{N} u_{ij}^2} \quad (5)$$

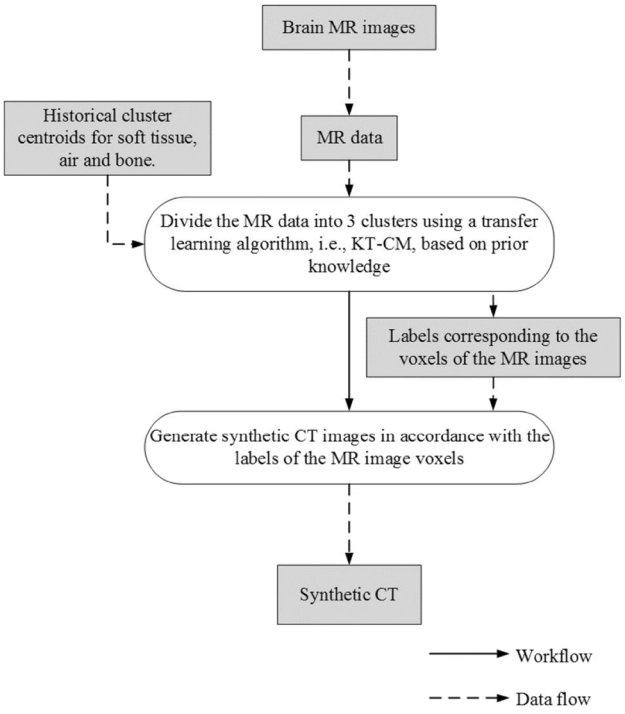

Fig. 1 Illustration of the data flow and workflow for synthetic CT generation

$$u_{ij} = \frac{1}{\left(2\left\|x_j - v_i\right\|^2 + 2\beta + 2\gamma\left\|\hat{v}_i - v_i\right\|^2 \sum_{k=1}^{C} \frac{1}{2\|x_j - v_k\|^2 + 2\beta + 2\gamma\|\hat{v}_k - v_k\|^2}\right)} \quad (6)$$

3 The proposed IC-G-MR method

Our proposed IC-G-MR method consists of two main phases. The first phase is synthetic CT generation based on the MR images; an advanced machine learning technique, i.e., transfer learning, is applied for this purpose. The second phase is image completion guided by synthetic-CT-based multimodal registration. Further details will be given below.

3.1 Phase 1: generation of synthetic CT results for the subjects

As the name of the proposed method implies, the process of synthetic CT generation somewhat affects the final image completion result. Importantly, the anatomical structure of the brain is relatively simple and clear, and tissue deformation due to organ movement or human respiration is extremely rare in this part of the body. Consequently, methods of synthetic CT generation for the brain are relatively mature.

Based on the characteristics of the brain, an advanced machine learning technique, i.e., transfer learning, is adopted

in our method to divide the MR data into three different tissue types: soft tissue, air and bone. With the tissue type results for all voxels of the MR images, satisfactory synthetic CT results can be successfully generated. Figure 1 illustrates the workflow and data flow for this phase.

Suppose that there are n subjects, each with three different brain MR sequences and CT scans. For all subjects, the MR images consist of three different types of MR sequences, i.e., fat, water and R2. During data pretreatment, with the corresponding mask for the MR images from all subjects, the MR data do not contain external air and can be represented in the form $Data_{MR} = [fat_{MR}, water_{MR}, R2_{MR}]$.

It is well known that transfer learning requires sufficient and advantageous prior knowledge, e.g., historical cluster centroids. In our method, the classical soft partition algorithm FCM is applied to obtain the historical centroids. More specifically, the historical cluster centroids are obtained by taking the averages of all subjects' preliminary clustering results from FCM, i.e., the soft tissue, air, and bone cluster centroids. Notably, air is associated with a very low signal in MR images. To ensure a reliable reference for the prior knowledge used in transfer learning, based on an extensive review of the related literature, the value of the historical cluster centroid for air is set to $1e-5$ (Schneider et al. 2000).

Using the historical cluster centroids, we divide the data again into three clusters corresponding to soft tissue, air and bone using a transfer learning algorithm, i.e., KT-CM. Thus, the tissue types of the voxels in the MR images are determined. Then, the specific CT values of the three tissue types mentioned above are used for synthetic CT generation.

3.2 Phase 2: image completion guided by synthetic-CT-based multimodal registration

The main idea of this phase is to replace the traditional input for multimodal registration with synthetic and real CT images. More generally, the original MR image completion problem here is converted into a problem of synthetic CT image completion. The synthetic CT results are generated using only MR data; therefore, the synthetic CT images are representative of the MR images. In this way, multimodal registration is approximately converted into monomodal registration.

Specifically, a non-rigid registration method based on local phase differences is adopted (Janssens et al. 2011). The non-rigid registration algorithm contains an iterative loop that mainly consists of four interconnected steps, i.e., deformation field computation, deformation field accumulation, deformation field regularization and image deformation. With the synthetic and real CT images as the input and the optimal deformation field as the output, the non-rigid registration method does not directly perform MR-to-CT registration. Instead, we apply the deformation field obtained by registering the real and synthetic CT images to the MR images to indirectly achieve multimodal registration. The framework of this phase is shown in Fig. 2.

When computing the deformation field for the input in our method, we use a filter to obtain the local phases of the fixed image and the moving image. The displacement D_u can be calculated by solving the optimization problem $\Theta_D(f,w) = \arg\min_{d\in\mathbb{R}^3} \sum_k \left[c_k\left(\rho\eta_k^T d - \Delta\phi_k\right)\right]^2$, where $c_k(x) = A_f(x;k)A_m(x;k)$ is the certainty mapping of the filter mentioned above, with $A_f(x;k)$ and $A_m(x;k)$ denoting the amplitudes of the fixed and moving images, respectively, which measure the adequacy of the fits between the images and the filter. Thus, c_k reflects the reliability of the field estimate for each voxel. Accordingly, the global certainty mapping, which is related to the quality of the estimation of Θ_D, can be expressed as $\Theta_c(f,w) = \sum_k c_k(x)$.

For the accumulation of the deformation field, some new tricks are adopted in our method. Let the deformation field be represented by a vector field $D \in v = \left\{V : \mathbb{R}^3 \to \mathbb{R}^3, x \mapsto V(x)\right\}$, and let $\Delta \overset{\Delta}{=} Id + D$ denote the deformation operation, where Id denotes the intensity deformation $Id(x) \overset{\Delta}{=} x$. Then, the accumulation process can be expressed as follows:

$$D_1 \oplus D_2 \overset{\Delta}{=} \Delta_1 \circ \Delta_2 - Id \tag{7}$$

where $\circ$ represents the common function composition operation, denoting the warping of two objects. The composition will remain diffeomorphic in the case of two diffeomorphic deformation fields.

For the field regularization process, the certainty map is used to adjust the importance of the targeted locations, i.e., higher significance is attached to locations with larger values in the certainty map. For regularization, the normalized convolution of the deformation field can be obtained using a Gaussian kernel. Suppose that we have a positive function h and that g denotes a filter; using g and h, the normalized convolution of the function s can be expressed as.

$$s * hg \overset{\Delta}{=} \frac{(hs) * g}{h * g} \tag{8}$$

The deformation field D_a and, subsequently, the certainty map are thus regularized by means of the operations expressed as follows:

$$\begin{aligned} \Psi_D\left(D_a, c_a\right) &= D_a * c_a g, \\ \Psi_c\left(c_a, c_a\right) &= c_a * c_a g. \end{aligned} \tag{9}$$

The regularized deformation field is used to warp the image to obtain the new moving image for the next iteration. Through multiple iterations, the deformation field is constantly optimized.

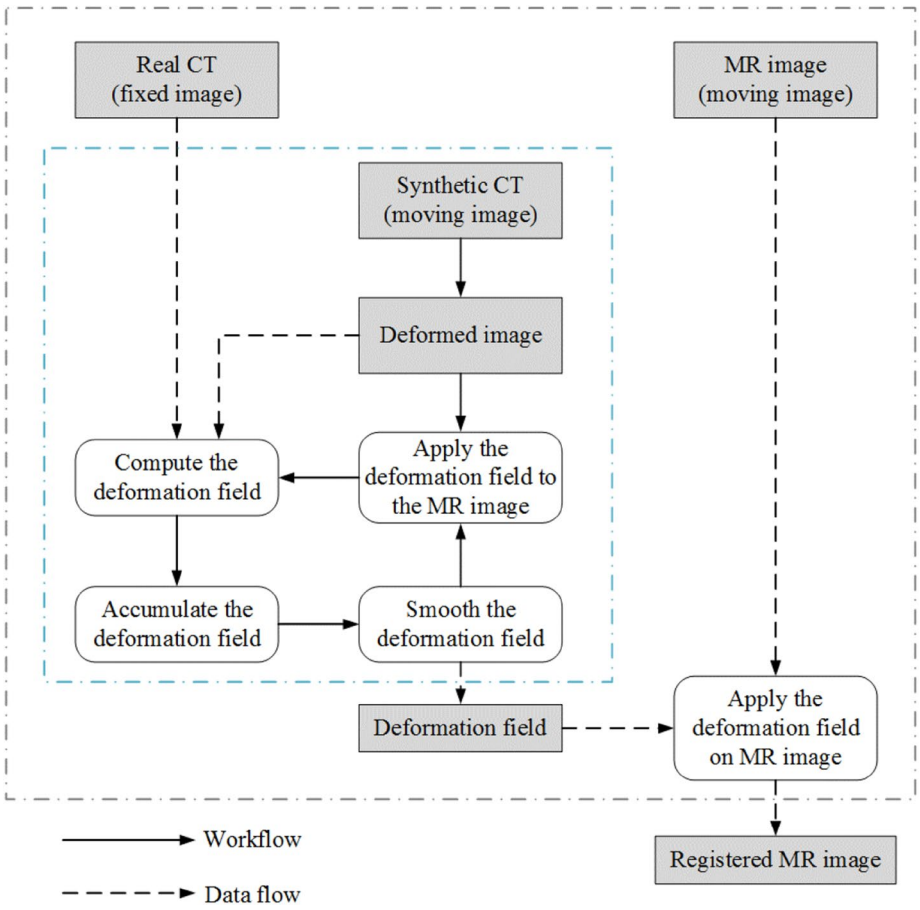

Fig. 2 Framework of multi-modal registration based on synthetic CT

Because a synthetic CT image that is generated completely on the basis of MR data is representative of the characteristics of the original MR image, the registration between a real CT image and this synthetic CT image will be approximately the same as the registration between the real CT image and the MR image, i.e., the MR image can be warped using the same deformation field found for the synthetic CT image. Thus, our method consists of two interrelated phases, i.e., synthetic CT generation and image completion guided by the registration between the synthetic and measured CT images. To some extent, the quality of the synthetic CT results generated in the first phase will affect the image completion results. Moreover, the time efficiency of the synthetic CT generation process must also be considered.

Finally, the computational complexity of our proposed IC-G-MR method is summarized in Table 1.

Table 1 Computational complexity of IC-G-MR

Phase	Computational complexity
Synthetic CT generation	$O(n)$
Registration	$O(N^2 \log N)$

4 Experiment and discussion

In this section, we illustrate the effectiveness of the proposed IC-G-MR method by means of an experimental validation.

4.1 Setup

In this experiment, data from nine subjects, including CT scans and three types of MR image sequences, e.g., fat, water and R2, were used. To simulate deformation and other unknown corruption of the images, we obtained two groups of MR data, i.e., warped MR images, labelled as sub1-9, and warped MR images with salt-and-pepper noise, labelled as sub1*-9*.

To demonstrate the advantages of our method, two traditional methods, i.e., the local-phase-difference-based method and the mutual-information-based method implemented in OpenREGGUI, an open-source image registration package, were selected for comparison.

Our experimental studies were carried out on a computer with an Intel i5-4590 3.3 GHz CPU, 12 GB of RAM, Microsoft Windows 10 (64-bit), and MATLAB 2016a.

4.2 Metrics for evaluation

To intuitively capture the effectiveness of our proposed method, three metrics are used in our research, e.g., the mutual information (MI), the sum of local phase differences (SLPD) and the cross-correlation (CC) (Yoo and Han 2009). Further details are shown below.

The SLPD is calculated as the sum of the local phase differences in all directions between two images. It is defined as

$$SLPD = \sum (\sin(\Delta\varphi)) \tag{10}$$

where $\Delta\varphi$ denotes a local phase difference between the two images.

The MI measures the mutual dependence between two images and is defined as

$$MI(f;m) = \sum_{f\in F}\sum_{m\in M} p(f,m)\log\left(\frac{p(f,m)}{p(x)p(y)}\right) \tag{11}$$

where $p(f,m)$ is the joint probability function of f and m and $p(f)$ and $p(m)$ are the marginal probability distribution functions of f and m, respectively.

The CC is a measure of the similarity between two series; it can also be regarded as a function of the displacement between them. For two continuous signals f and g, the CC is defined as

$$CC:\ (f*g)(\tau) \triangleq \int_{-\infty}^{\infty} \overline{f(t)}g(t+\tau)dt \tag{12}$$

where $\overline{f(t)}$ denotes the complex conjugate of $f(t)$ and corresponds to the displacement.

4.3 Results and discussion

To illustrate the effectiveness of our method, we list the values of the three metrics introduced above for each subject in Table 2. The performance curves of the three methods corresponding to each subject are also shown in Fig. 3.

The synthetic CT generation phase is an important component of our method. In MR images, bone and air both generate low signals, and it is difficult to differentiate one of them from the other using classical clustering algorithms. The introduction of transfer learning in our method takes great advantage of prior knowledge, allowing the air in the MR images to be distinguished relatively accurately. Thus, air and bone regions can be effectively separated from each other, and the remaining tissue type, i.e., soft tissue, can be more easily distinguished. Profiting from the incorporation of this machine learning technique, our method can obtain better synthetic CT results for the brain. Figure 4 shows some synthetic CT images generated via KT-CM and FCM. In addition, we use the mean absolute prediction deviation

Table 2 Performance comparison between the proposed IC-G-MR method and other methods

Sub	MI			SLPD			CC		
	IC-G-MR	Local-phase-based	MI-based	IC-G-MR	Local-phase-based	MI-based	IC-G-MR	Local-phase-based	MI-based
1	**0.9676**	0.9631	0.9623	**3.89E+05**	4.62E+05	4.73E+05	**0.0303**	0.0234	0.0236
2	**0.9580**	0.9568	0.9568	**5.19E+05**	5.84E+05	5.89E+05	**0.0254**	0.0193	0.0198
3	**0.9677**	0.9630	0.9639	**4.15E+05**	4.85E+05	4.77E+05	**0.0230**	0.0156	0.0162
4	**0.9685**	0.9639	0.9640	**4.13E+05**	4.73E+05	4.76E+05	**0.0275**	0.0210	0.0211
5	**0.9654**	0.9598	0.9596	**4.49E+05**	5.30E+05	5.55E+05	**0.0274**	0.0211	0.0203
6	**0.9596**	0.9550	0.9553	**4.89E+05**	5.67E+05	5.63E+05	**0.0232**	0.0181	0.0179
7	**0.9712**	0.9663	0.9659	**3.68E+05**	4.41E+05	4.38E+05	**0.0239**	0.0163	0.0168
8	**0.9676**	0.9628	0.9622	**4.10E+05**	5.01E+05	4.95E+05	**0.0233**	0.0163	0.0176
9	**0.9612**	0.9556	0.9564	**4.46E+05**	5.52E+05	5.45E+05	**0.0353**	0.0281	0.0280
1*	**0.9678**	0.9633	0.9623	**3.85E+05**	4.59E+05	4.78E+05	**0.0298**	0.0239	0.0240
2*	**0.9572**	0.9570	0.9570	**5.39E+05**	5.75E+05	5.73E+05	**0.0238**	0.0201	0.0205
3*	**0.9676**	0.9633	0.9637	**4.14E+05**	4.84E+05	4.87E+05	**0.0204**	0.0165	0.0169
4*	**0.9679**	0.9642	0.9641	**4.26E+05**	4.70E+05	4.78E+05	**0.0275**	0.0217	0.0218
5*	**0.9637**	0.9601	0.9598	**4.70E+05**	5.34E+05	5.45E+05	**0.0298**	0.0221	0.0214
6*	0.9543	0.9560	**0.9558**	**5.45E+05**	5.69E+05	5.69E+05	0.0182	0.0213	**0.0221**
7*	**0.9707**	0.9664	0.9663	**3.71E+05**	4.36E+05	4.39E+05	**0.0224**	0.0168	0.0173
8*	**0.9668**	0.9631	0.9623	**4.12E+05**	4.99E+05	4.89E+05	**0.0220**	0.0168	0.0181
9*	**0.9607**	0.9558	0.9567	**4.75E+05**	5.57E+05	5.40E+05	**0.0391**	0.0286	0.0284

Bold entries denote the best results obtained by the adopted methods

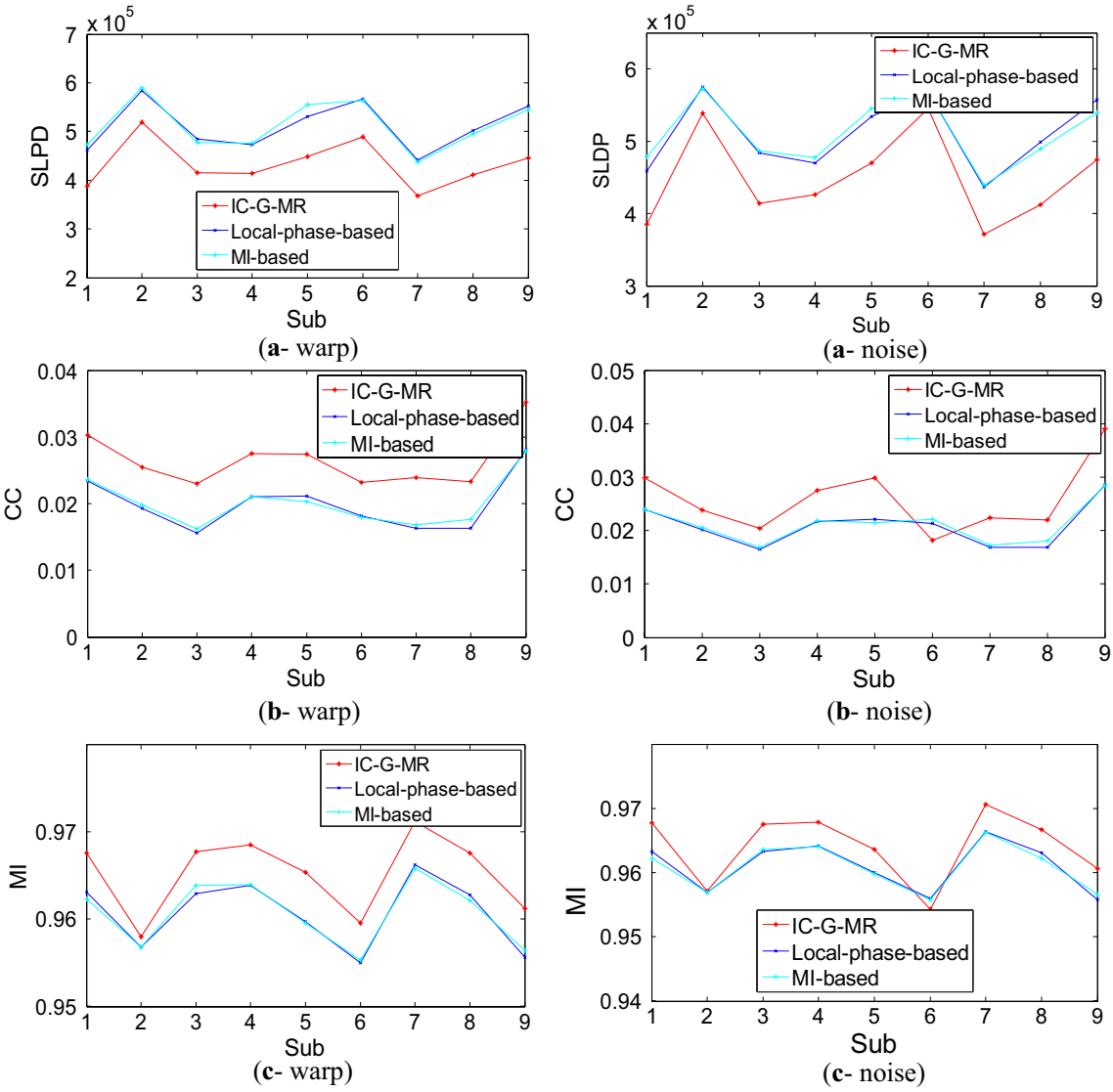

Fig. 3 Performance curves of three methods; the proposed IC-G-MR method has a lower sum of local phase differences (SLPD), a higher mutual information (MI) and a higher cross-correlation (CC) than the two traditional methods, i.e., the local-phase-based method and the MI-based method, do

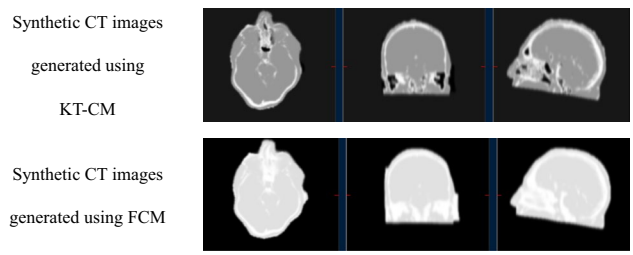

Fig. 4 Synthetic CT images generated using KT-CM and FCM for sub2

Table 3 Performance comparison between KT-CM and FCM

Sub	MAPD		R	
	FCM	KT-CM	FCM	KT-CM
1	191.28	**136.05**	0.5725	**0.8010**
2	205.82	**153.69**	0.4602	**0.7362**
3	190.70	**138.26**	0.5985	**0.7899**
4	222.61	**155.76**	0.5700	**0.8021**
5	194.15	**173.66**	0.5613	**0.7473**
6	181.72	**146.03**	0.5766	**0.7602**
7	201.95	**130.08**	0.5548	**0.8147**
8	188.23	**133.10**	0.5027	**0.7430**
9	213.12	**147.51**	0.5917	**0.8323**

Bold entries denote the best results obtained by the adopted methods

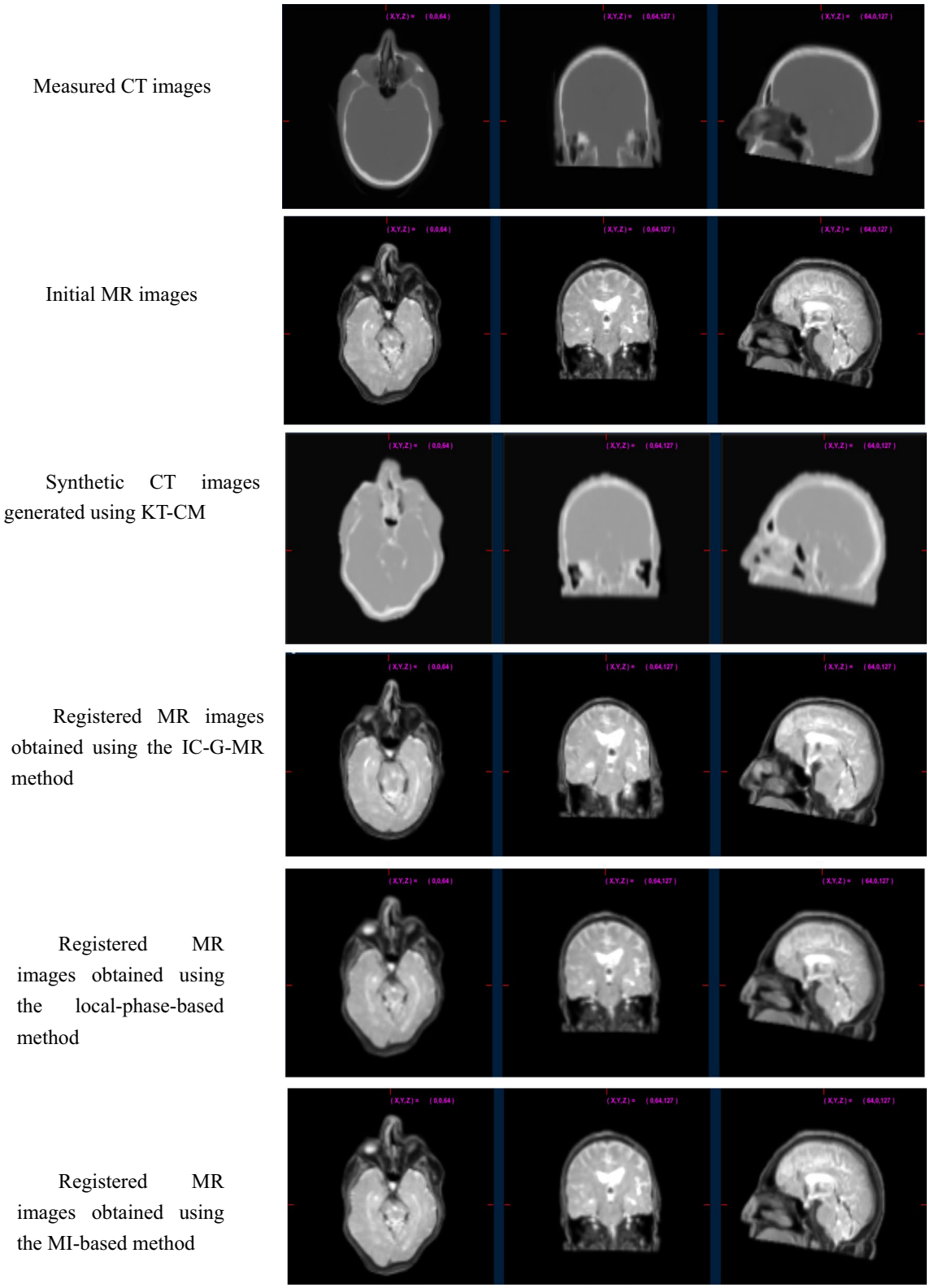

Fig. 5 Registered MR images for sub2 obtained using the method introduced in Sect. 3 and the two methods considered for comparison

Table 4 Time consumption of the three methods

Sub	IC-G-MR			Local-phase-based	MI-based
	Synthetic CT generation (s)	Registration (s)	Total time (s)	Total time (s)	Total time (s)
1	26	84	**110**	665	4296
2	26	84	**110**	680	4376
3	26	90	**116**	695	4339
4	26	89	**115**	691	4431
5	26	87	**113**	691	4429
6	26	84	**110**	649	4218
7	26	82	**108**	697	4230
8	26	85	**111**	708	4119
9	26	99	**115**	692	4297

Bold entries denote the best results obtained by the adopted methods

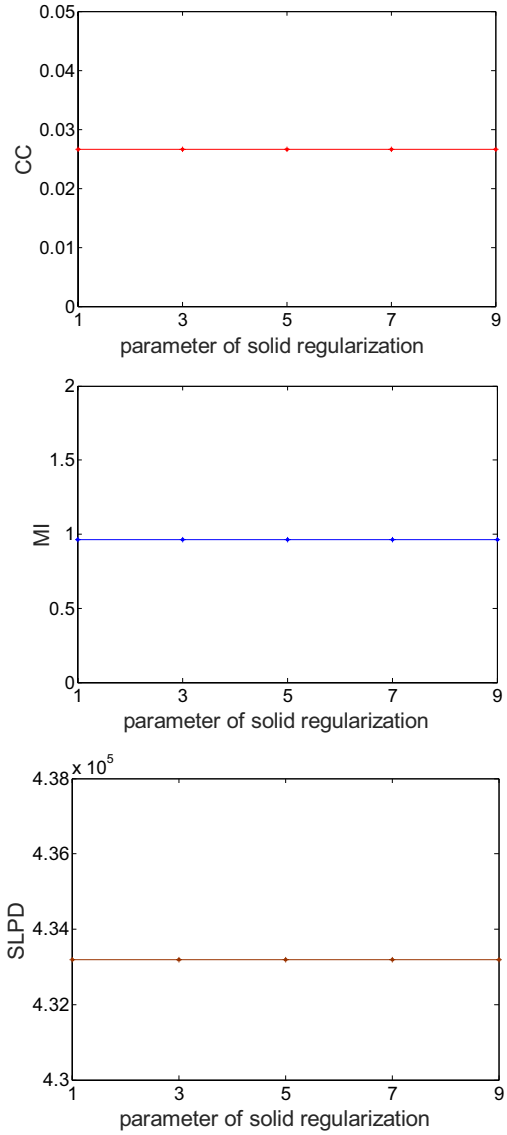

Fig. 6 Parameter robustness of the IC-G-MR method

(MAPD) and the R value to evaluate the performance of KT-CM and FCM in synthetic CT generation. The specific values of these metrics are listed in Table 3.

With synthetic CT generation, the problem of multimodal registration between MR and CT images can be easily converted into a problem of monomodal registration between real and synthetic CT images. That is, the proposed IC-G-MR method uses synthetic CT images as an intermediary in the traditional multimodal registration process, thus successfully addressing the challenges of multimodal registration that are caused by the significant differences between images of different modes. Ultimately, our proposed method enables the completion of problematic MR images. Experiments indicate that under the guidance provided by the multimodal registration between normal CT images and problematic MR images, the proposed method can achieve superior performance in brain MR image completion (see Fig. 5).

It should be noted that our proposed method is intended to address a clinical problem. In clinical applications, time is life. Therefore, it is important to discuss the time consumption of our proposed IC-G-MR method. To evaluate the time efficiency of the three methods considered in this study, we calculated the total time costs of these methods, which are listed in Table 4. Our method consists of two interrelated phases, i.e., synthetic CT generation and registration. The time cost of our method is less than approximately 2 min, whereas the two methods considered for comparison take more than 10 min, or even longer than an hour. Thus, our method obviously consumes less time and obtains better results than either of these methods.

In addition, the parameter sensitivity of our method is shown in Fig. 6. We primarily analyse the sensitivity to the parameter used in the solid regularization process in the registration phase. Our method shows great robustness to this parameter.

These experiments on multiple sets of medical brain images demonstrate that our method can effectively repair

deformed MR images. However, the IC-G-MR method has some limitations regarding its potential application scenarios. Specifically, our method requires normal CT scans from the same patient to serve as a guide to enable indirect multimodal registration between the MR and CT images and thus achieve successful image completion. Nevertheless, compared with the existing methods of multimodal registration, our method exhibits clear superiority.

5 Conclusion

Our study focused on the problem of brain MR image completion based on corresponding normal CT images. For this purpose, we proposed the IC-G-MR method based on transfer learning for synthetic CT generation and subsequent indirect multimodal registration. Our proposed method can generate satisfactory synthetic CT results for the brain using only MR images. With guidance from synthetic-CT-based multimodal registration for MR image completion, our method can perform better than other existing multimodal registration methods.

Acknowledgements This work was supported in part by the National Natural Science Foundation of China under Grants 61702225 and 61772241, by the 2018 Six Talent Peaks Project of Jiangsu Province under Grant XYDXX-127, by a Science and Technology Demonstration Project for the Social Development of Wuxi under Grant WX18IVJN002, and by the Jiangsu Committee of Health under Grant H2018071.

References

Ahmad S, Khan MF (2018) Multimodal non-rigid image registration based on elastodynamics. Vis Comput 34(1):21–27

Alafeef M, Fraiwan M (2019) On the diagnosis of idiopathic Parkinson's disease using continuous wavelet transform complex plot. J Ambient Intell Humanized Comput 10(7):2805–2815

Alvén J, Norlén A, Enqvist O, Kahl F (2016) Überatlas: fast and robust registration for multi-atlas segmentation. Pattern Recogn Lett 80:249–255

Akhbardeh A, Parekth VS, Jacobs MA (2015) TU-CD-BRA-01: A novel 3D registration method for multiparametric radiological. Images Medical physics 42(6Part32):3605–3606

Chen Q, Li G, Xie L, Xiao Q, Xiao M (2019) Structure guided image completion using texture synthesis and region segmentation. Optik 185:896–909

Farjam R, Tyagi N, Deasy JO, Hunt MA (2019) Dosimetric evaluation of an atlas-based synthetic CT generation approach for MR-only radiotherapy of pelvis anatomy. J Appl Clin Med Phys 20(1):101–109

Fernandez-de-Manuel L, Wollny G, Kybic J, Jimenez-Carretero D, Tellado JM, Ramon E, Ledesma-Carbayo MJ (2014) Organ-focused mutual information for nonrigid multimodal registration of liver CT and Gd–EOB–DTPA-enhanced MRI. Med Image Anal 18(1):22–35

Guo K, Cao R, Kui X, Ma J, Kang J, Chi T (2019) LCC: towards efficient label completion and correction for supervised medical image learning in smart diagnosis. J Netw Comput Appl 133:51–59

Han B, Han Y, Gao X, Zhang L (2018) Boundary constraint factor embedded localizing active contour model for medical image segmentation. J Ambient Intell Human Comput. https://doi.org/10.1007/s12652-018-0978-x

Hofmann M, Steinke F, Scheel V, Charpiat G, Farquhar J, Aschoff P, Pichler BJ (2008) MRI-based attenuation correction for PET/MRI: a novel approach combining pattern recognition and atlas registration. J Nucl Med 49(11):1875–1883

Iizuka S, Simo-Serra E, Ishikawa H (2017) Globally and locally consistent image completion. ACM Trans Graph (ToG) 36(4):107

Janssens G, Jacques L, de Xivry JO, Geets X, Macq B (2011) Diffeomorphic registration of images with variable contrast enhancement. J Biomed Imaging 2011:3

Keereman V, Fierens Y, Broux T, De Deene Y, Lonneux M, Vandenberghe S (2010) MRI-based attenuation correction for PET/MRI using ultrashort echo time sequences. J Nucl Med 51(5):812–818

Kops ER, Herzog H (2008) Template based attenuation correction for PET in MR-PET scanners. In: 2008 IEEE nuclear science symposium conference record pp 3786–3789

Lee D, Nam WH, Lee JY, Ra JB (2010) Non-rigid registration between 3D ultrasound and CT images of the liver based on intensity and gradient information. Phys Med Biol 56(1):117

Manchanda M, Sharma R (2018) An improved multimodal medical image fusion algorithm based on fuzzy transform. J Vis Commun Image Represent 51:76–94

Qian P, Sun S, Jiang Y, Su KH, Ni T, Wang S, JrRF Muzic (2016) Cross-domain, soft-partition clustering with diversity measure and knowledge reference. Pattern Recogn 50:155–177

Raja NSM, Fernandes SL, Dey N, Satapathy SC, Rajinikanth V (2018) Contrast enhanced medical MRI evaluation using Tsallis entropy and region growing segmentation. J Ambient Intell Human Comput. https://doi.org/10.1007/s12652-018-0854-8

Schneider W, Bortfeld T, Schlegel W (2000) Correlation between CT numbers and tissue parameters needed for Monte Carlo simulations of clinical dose distributions. Phys Med Biol 45(2):459

Sharif M, Tanvir U, Munir EU, Khan MA, Yasmin M (2018) Brain tumor segmentation and classification by improved binomial thresholding and multi-features selection. J Ambient Intell Human Comput. https://doi.org/10.1007/s12652-018-1075-x

Tao X, Wang R, Chang R, Li C (2019) Density-sensitive fuzzy kernel maximum entropy clustering algorithm. Knowl-Based Syst 166:42–57

Wen J, Tian Y, Yehang SHOU, Yongchuan T, Weiwei HU (2018) Improved evidential fuzzy c-means method. J Syst Eng Electron 29(1):187–195

Xue C, Tang FH (2014) An adaptive patient specific deformable registration for breast images of positron emission tomography and magnetic resonance imaging using finite element approach. In: Medical imaging 2014: image processing, Vol. 90343H, International Society for Optics and Photonics, 21 March 2014, pp 1–6. https://doi.org/10.1117/12.2043252

Yang L, Guo BL, Ni W (2008) Multimodality medical image fusion based on multiscale geometric analysis of contourlet transform. Neurocomputing 72(1–3):203–211

Yoo JC, Han TH (2009) Fast normalized cross-correlation. Circuits Syst Signal Processing 28(6):819

Zaidi H, Montandon ML, Slosman DO (2003) Magnetic resonance imaging-guided attenuation and scatter corrections in three-dimensional brain positron emission tomography. Med Phys 30(5):937–948